Atmospheric Environment 272 (2022) 118943

Contents lists available at ScienceDirect

Atmospheric Environment

journal homepage: www.elsevier.com/locate/atmosenv

Changes in aerosol particle composition during sea fog formation events in the sea ice regions of the Arctic Ocean

Shuhui Zhao [a,b], Jinpei Yan [a,b,*], Qi Lin [a,b], Lei Yao [c,d], Keyhong Park [e], Jinyoung Jung [e], Liqi Chen [a,b], Suqing Xu [a,b], Meiping Sun [f], Shanshan Wang [a,b], Hang Yang [a,b], Jun Shi [a,b], Miming Zhang [a,b], Heng Sun [a,b]

[a] Key Laboratory of Global Change and Marine Atmospheric Chemistry, Ministry of Natural Resources, Xiamen, 361005, China
[b] Third Institute of Oceanography, Ministry of Natural Resources, Xiamen, 361005, China
[c] Shanghai Key Laboratory of Atmospheric Particle Pollution and Prevention (LAP3), Department of Environmental Science and Engineering, Fudan University, Shanghai 200438, China
[d] Institute for Atmospheric and Earth System Research, Faculty of Science, University of Helsinki, Helsinki, Finland
[e] Division of Polar Ocean Science, Korea Polar Research Institute, 26 Songdomirae-ro, Yeonsu-gu, Incheon, 21990, South Korea
[f] College of Geography and Environment Sciences, Northwest Normal University, Lanzhou, 730070, China

HIGHLIGHTS

- Hourly real-time measurements of aerosol compositions were conducted during sea fog events in the Arctic Ocean.
- Sea salt aerosol concentrations increased before sea fog formed, but decreased dramatically when sea fog formation began.
- Non-sea-salt sulfate (nss-SO_4^{2-}) concentrations remained consistently high during sea fog formation processes.
- Condensation may be the primary factor leading to the reduction of sea salt ions during the sea fog periods.

ARTICLE INFO

Keywords:
Sea fog
Aerosol
Arctic ocean
Sea salt aerosol
Non-sea salt sulfate (nss-SO_4^{2-})

ABSTRACT

Water soluble ions (WSIs) of aerosol particles is one of the important parameters to study the aerosol-fog interactions. To study the changes of aerosol WSIs during sea fog events, hourly real-time measurements of WSIs (Na^+, K^+, Mg^{2+}, Ca^{2+}, MSA^-, Cl^-, NO_3^-, and SO_4^{2-}) in total suspended aerosol particles (TSP) were conducted in the atmosphere over Arctic Ocean ice floe regions from August 1 to 12, 2017, when the sea fog events were frequently observed. There were significant differences in Na^+, Cl^-, Mg^{2+}, methanesulfonic acid (MSA^-), sea salt sulfate (ss-SO_4^{2}) and non-sea salt sulfate (nss-SO_4^{2-}) ions during sea fog events vs. non-sea fog periods. The mass concentrations of sea salt ions, such as Na^+, Mg^{2+}, Cl^- and ss-SO_4^{2-}, clearly increased before the occurrence of sea fog and then decreased substantially with the formation of sea fog; however, nss-SO_4^{2-} levels did not decrease but remained high during the sea fog processes. These results suggest that sea salt aerosol particles were more likely to serve as condensation nuclei for fog and could be more effectively removed by sea fog than nss-SO_4^{2-} particles. MSA^- only combined with sea salt particles, which were likely to serve as condensation nuclei and be removed by sea fog. Condensation may be the primary factor leading to the reduction of sea salt ions during the sea fog periods, while other factors like the presence of dense sea ice and long-range transport input may also affect the decreasing rate.

1. Introduction

Fog is a ubiquitous atmospheric phenomenon in which horizontal visibility is reduced to below 1 km due to suspended water droplets or ice crystals near the Earth's surface (Gultepe et al., 2007). Low visibility caused by fog can severely influence human activities, leading to

* Corresponding author. Third Institute of Oceanography, Ministry of Natural Resources, Key Laboratory of Global Change and Marine-Atmospheric Chemistry, Daxue road 178#, Siming district, Xiamen, 361005, China.
E-mail address: jpyan@tio.org.cn (J. Yan).

https://doi.org/10.1016/j.atmosenv.2022.118943
Received 1 October 2021; Received in revised form 1 January 2022; Accepted 4 January 2022
Available online 7 January 2022

numerous traffic accidents and delays. The loss of life and damage to property caused by fog highlight the significance of fog monitoring and prediction (Shin and Kim, 2018). However, due to our incomplete understanding of fog processes, it is still difficult to predict fog, and there continues to be significant uncertainty in climate modeling (IPCC, 2013). Fog processes involve droplet microphysics, aerosol chemistry, radiation, turbulence, large- and small-scale dynamics, and surface conditions (Gultepe et al., 2007). The complexity of aerosol-fog interdependence is one of the important aspects of the understanding of fog processes (Gultepe et al., 2007). As the activation, diffusion and growth of fog droplets depend on the physico-chemical character of the ambient aerosols, intricate relationships exist between aerosols and fog characteristics: 1) aerosol particles can act as condensation nuclei to promote the formation and evolution of fog; 2) the physical and chemical characteristics of aerosols (e.g., number concentration, particle size, and chemical composition) have a great influence on the formation of fog; and 3) the fog processes can substantially alter the evolution of aerosols (e.g., new particle formation, secondary conversion, and removal) (Gultepe et al., 2007; Biswas et al., 2008; Li et al., 2011). Thus, to improve fog forecasting, it is crucial to understand aerosol-fog interactions.

Previous studies on fog and aerosol-fog interactions have been conducted all over the world; however, most studies focused on land fog (e.g. Bott, 1991; Yuskiewicz et al., 1998; Mohan and Payra, 2006; Aikawa et al., 2007; Niu et al., 2010; Fan et al., 2010; Ian et al., 2018; Brege et al., 2018; Jia et al., 2019; Tsai et al., 2021), and little attention was given to sea fog (e.g. Sasakawa and Uematsu, 2002; Sasakawa et al., 2003; Pant et al., 2010; Sheng et al., 2011). Sea fog is a hazardous atmospheric phenomenon that occurs within the marine atmospheric boundary layer (Yang and Gao, 2020). It usually forms as a result of the advection of warm and moist air masses that pass over cold ocean surfaces and cool to a sufficiently low saturation temperature (Cotton and Anthes, 1989; Koračin et al., 2001; Sasakawa et al., 2003; Gultepe et al., 2007; Gilson et al., 2018). Low visibility caused by sea fog can seriously affect marine activities such as navigation and aviation and result in transportation risk. To mitigate transportation hazards and improve weather and visibility forecasting, sea fog research is vital (Gultepe et al., 2007; Koračin and Dorman, 2017; Yang and Gao, 2020). Over polar ocean water, sea fog is expected to increase in frequency due to warmer oceans and the declining extent of seasonal sea ice (Deser et al., 2010; Eastman and Warren, 2010; Palm et al., 2010; Vavrus et al., 2011). One previous study found that the Arctic Ocean and North Pacific Ocean regions at latitudes >40° have a high sea fog frequency with a maximum of 50% in summertime (Wang, 1985). Arctic sea fog peaks when sea ice breaks apart, and most frequently occurs throughout the Arctic melt season (Tjernström et al., 2012, 2015; Gilson et al., 2018). However, research on the interactions between sea fog and aerosol particles in the Arctic region is rather limited.

Sea fog and aerosol chemistry were investigated during the 8th Chinese National Arctic Research Expedition (CHINARE) from July 20 to October 7, 2017. According to the statistical data obtained from an automatic weather station, sea fog was observed on 66 d, i.e., approximately 82.5% of the whole Expedition, while according to manual observations, there were 44 d of sea fog, accounting for 55% of the investigation (Chen et al., 2019). The different statistical results for the number of days of sea fog are because the automatic weather station misjudged periods of low visibility, e.g., rainy days, as foggy days, while manual observations were limited by the observation time, which led to omissions. However, both sets of observations and data indicated that sea fog occurred frequently during the Expedition. In this study, aerosol chemistry was investigated over the Arctic Ocean ice floe regions from August 1 to 12, 2017, during which time sea fog events were frequently observed. The chemical compositions of the aerosol particles acting as condensation nuclei determine the initial compositions of the fog droplets (Sasakawa et al., 2003; Yue et al., 2014); whereas, higher relative humidity during fog conditions enhanced uptake and scavenging of soluble aerosol species in fog droplets. Thus, the water soluble ions (WSIs) of aerosol particles is one of the important parameters to study the aerosol-fog interactions. To study the changes of aerosol WSIs during sea fog events, a recently commercialized semi continuous in situ gas and aerosol composition (IGAC) monitoring system and ion chromatography were deployed for the high-resolution time-resolved characterization of atmospheric aerosol particles during sea fog processes. This study helps to improve current understanding of the relationship between sea fog processes and aerosol chemistry over the Arctic Ocean, and the results can be used to understand sea fog formation and improve the assessment of ocean-atmosphere interactions and their impact on the climate and ecological environment of the Arctic.

2. Materials and method

2.1. Observation period and regions

The 8th CHINARE Expedition was conducted from July 20 to October 7, 2017. The research vessel (R/V) Xuelong, an icebreaker, set sail from Shanghai, China, crossed the East China Sea, the Sea of Japan, the Sea of Okhotsk, the Northwest Pacific Ocean, the Bering Sea, and the Arctic Ocean, circled the Arctic Polar in a clockwise direction, and finally returned to Shanghai; the whole cruise was shown in Fig. 1a. This was the first time that the Xuelong icebreaker voyaged through the Arctic Ocean along the Northwest Passage. This study focused on the Arctic Ocean during the period from August 1 to 12 (as shown in Fig. 1b). During this period, intensive sea fog observation was conducted by the researchers from Chinese academy of meteorological science (Chen et al., 2019).

2.2. Instruments and data analysis

During the 8th CHINARE cruise, an in situ gas and aerosol composition monitoring system (IGAC, Model S-611, Machine Shop, Fortelice International Co. Ltd.) and two online ion chromatographs (Dionex ICS-1100) were deployed hourly to make high-resolution measurements of the water soluble ions (WSIs) in atmospheric aerosol particles. A detailed description and explanation of the operation of the IGAC can be found in Young et al. (2016), Tian et al. (2017), and Yan et al. (2020a). Similar to the study by Tian et al. (2019), the instruments were installed in a laboratory on the first deck of the R/V, ambient air was drawn into the system through a 3/4-inch silicone tube at a flow rate of 1 m^3/h. The sampling inlet with a total suspended particulate (TSP) sampler was located at~8 m above sea level on the second floor and influence from smoke emitted by the chimney that rested on top of the R/V was limited. The gases and aerosol particles were separated and streamed into liquid effluent for extraction. In this study, we focused on the soluble ions Cl^-, NO_3^-, SO_4^{2-}, MSA^-, Na^+, K^+, Mg^{2+}, and Ca^{2+} in the TSP; their detection limits in aqueous solution were 0.03 μg/L, 0.05 μg/L, 0.006 μg/L, 0.05 μg/L, 0.03 μg/L, 0.015 μg/L, 0.007 μg/L, and 0.012 μg/L, respectively. Non-sea-salt sulfate (nss-SO_4^{2-}) concentrations were calculated according to the following equation: [nss-SO_4^{2-}] = [SO_4^{2-}]- [Na^+] × 0.25, where 0.25 was the mass ratio of sulfate and sodium in seawater (Millero and Sohn, 1992). Sea salt sulfate (ss-SO_4^{2-}) concentrations were obtained by calculating [SO_4^{2-}] - [nss-SO_4^{2-}].

Meteorological parameters such as the wind speed, wind direction, air temperature, precipitation, relative humidity (RH) and visibility were recorded using automatic weather stations (AWS, Vaisala 500) installed on the R/V Xuelong. Sea ice concentration data from the daily 3.125-km AMSR2 dataset (available at https://seaice.uni-bremen.de) (Spreen et al., 2008).

To identify potential transport pathways and possible source regions of aerosols over the Arctic Ocean, air mass back-trajectories were calculated by the Hybrid Single-Particle Lagrangian Integrated Trajectory (HYSPLIT) model of the Air Resources Laboratory of the National

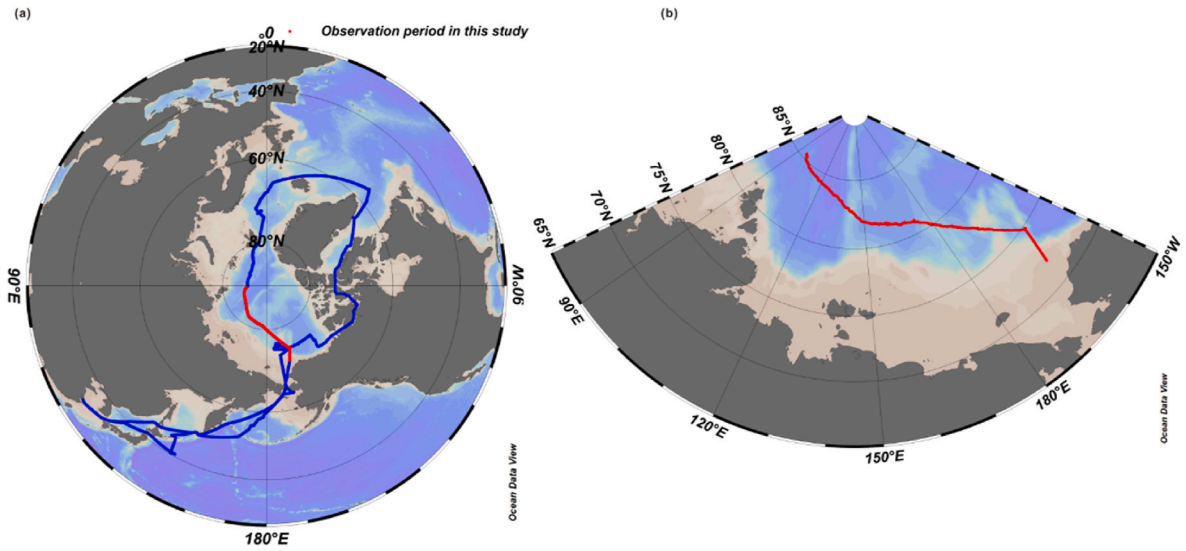

Fig. 1. a) Cruise of the 8th CHINARE (Red line represents the observation period in this study); b) Enlarged view of the study period. (For interpretation of the references to color in this figure legend, the reader is referred to the Web version of this article.)

Oceanic and Atmospheric Administration (NOAA) (Draxler and Rolph, 2003). Meteorological field data used to run the model were obtained from the US National Centers for Environmental Prediction (NCEP). The vertical motion was calculated using the vertical velocity in the meteorological model. The model output was a set of latitude–longitude coordinates of the estimated position of the air parcel with a 6-h time interval and pressure vertical coordinate. In this study, 72-h backward air trajectories were simulated with a daily resolution.

3. Results and discussion

3.1. Characteristics of the aerosol WSIs and meteorological parameters during the observation periods

Fig. 2 shows the temporal variations in the meteorological parameters and mass concentrations of some representative ions during the whole observation period. Most of the time, except for several hours, the RH was almost 100%, which indicated that the humidity of the atmospheric environment over the Arctic Ocean ice floes was very high. Air temperatures significantly decreased on August 1' when the ship was sailing towards the area with floating ice, according to the cruise route. Ice floes first appeared on August 2 (00:00). On August 3, the ship entered an area where there was dense floating ice and the sea ice density was greater than 70% (as shown in Figs. 1 and 3a). Thus, the air temperature decreased obviously and remained at or below 0 °C. Visibility, together with RH, is typically used to distinguish fog and haze. Low visibility combined with high RH (above 90%) usually identifies as a fog event. According to the definitions of meteorology, dense fog, heavy fog, fog and light fog were identified by horizontal visibility< 0.2 km, < 0.5 km, < 1 km, and <10 km, respectively. Precipitation or snow

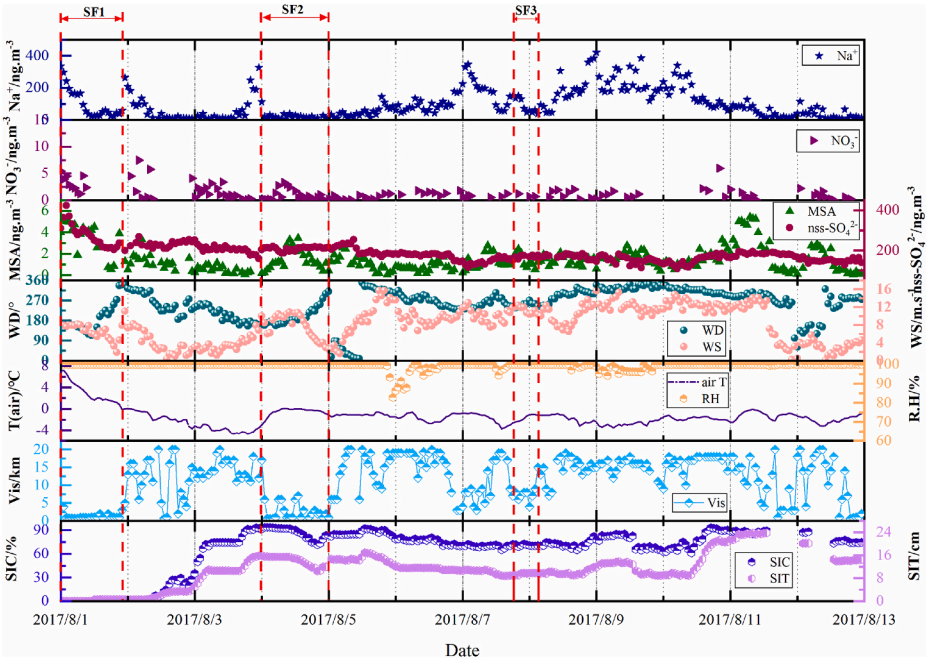

Fig. 2. Mass concentrations of particulate Na^+, MSA^-, NO_3^- and nss-SO_4^{2-}, and meteorological parameters during August 1st to 12th, 2017 over the Arctic Ocean (SF1-SF3 represent three sea fog events, SIC represent sea ice concentration, while SIT represent sea ice thickness).

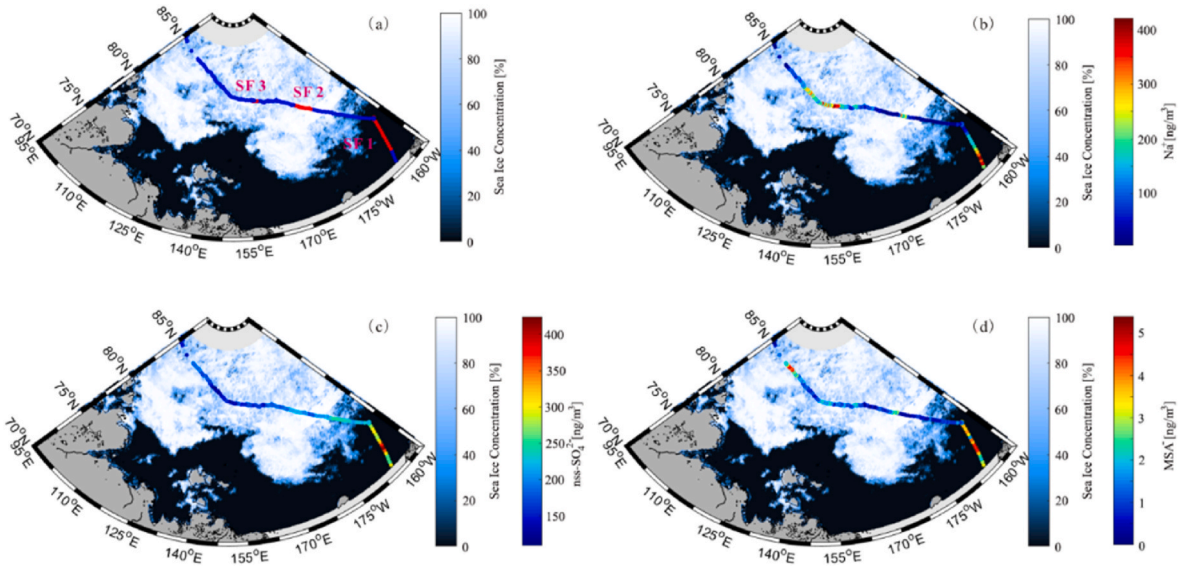

Fig. 3. Spatial distributions of a) sea fog processes (color bar represents the sea ice concentrations) and aerosol WSIs b) Na^+, c) nss-SO_4^{2-} and d) MSA^- (color bars represent the mass concentrations of the ions) over the Arctic Ocean. (For interpretation of the references to color in this figure legend, the reader is referred to the Web version of this article.)

events can also be associated with low visibility; thus, detailed information on the meteorological parameters was carefully checked. During this observation period, the visibilities ranged from 0.6 km to 20 km. Most of the time, visibilities were greater than 10 km; however, the visibility was very low (close to 0 km) for several hours or days. Chen et al. (2019) reported that three types of sea fog occurred over the Arctic Ocean, advection fog, radiation fog and steam fog; from August 1 to 12, there were approximately 10 sea fog events, including 4 advection fog events, 5 radiation fog events and 1 steam fog event (Table S1). The low visibility caused by advection fog persists for a long time, sometimes for even more than 24 h. According to a study by Chen et al. (2019), we divided the observation period into: the sea fog (SF) period and the non-sea fog (NSF) period. Changes in aerosol WSIs during three long-term advection fog events, named SF1, SF2 and SF3 (shown in Fig. 2), are discussed in detail.

The ocean is a major natural source of sea salt aerosol particles and other biogenic marine aerosol particles. Ions are classified into two categories, primary sea salt (original) ions and secondary (conversion) ions, according to correlation coefficients (listed in Table S2). Na^+, Cl^-, and Mg^{2+}, typically used as markers of sea salt in the marine atmosphere are mainly primary sea salt (original) ions. Concentrations of K^+ and Ca^{2+} exhibited a significant positive correlation with Na^+ and Cl^-indicating that they may also mainly originate from sea salts. Jung et al. (2013) reported that over the subarctic western North Pacific Ocean, most of the Mg^{2+}, K^+ and Ca^{2+} present in aerosols and sea fog water originated in sea salt particles. Dimethyl sulfide (DMS), released by phytoplankton, is an important source of sulfur in the marine atmosphere boundary layer (Bates et al., 1992; Jung et al., 2014; Yan et al., 2020b). The two major oxidation products of DMS are MSA and sulfate (usually called nss-SO_4^{2-}). In the marine atmosphere, MSA mainly originates from the oxidation of DMS and is typically used as a marker of biogenic origin, while SO_4^{2-} has several other sources, including oceanic spray (ss-SO_4^{2-}) and volcanic and anthropogenic inputs (nss-SO_4^{2-}), which may be obtained from the conversion of SO_2. Similarly, NO_3^- may result from the conversion of NOx. Thus, nss-SO_4^{2-}, NO_3^- and MSA^- were mainly secondary (conversion) ions. In Fig. 2, Na^+ was used to represent the sea salt particles, while MSA^-, NO_3^-, and nss-SO_4^{2-} represented the biogenic and secondary conversation particles. The average mass fractions of theses represent ions during the whole period were 23.6%, 0.4%, 0.3% and 44.5% respectively (as shown in Fig. S1). The mass concentrations of Na^+ during the observation period ranged from approximately 5 ng m^{-3} to over 400 ng m^{-3}. The highest values of Na^+ were observed during periods of several hours on August 1, 2, 3, 7, and 9, when, in most cases, wind speeds were higher than 8 m/s. Sea salt aerosols originating from broken sea bubbles usually increased with increasing wind speed. MSA^- concentrations were much lower than those of Na^+. Higher concentrations of MSA^- were found on August 1, 4 and 11. MSA^- concentrations were lower than 2 ng m^{-3} most of the time. Similarly, NO_3^- concentrations were low most of the time; the highest concentration of NO_3^- was observed on August 2. Unlike MSA^- and NO_3^-, the mass concentrations of nss-SO_4^{2-} were much higher and ranged from approximately 100 ng m^{-3} to 400 ng m^{-3} during the whole period. According to Fig. 2, the nss-SO_4^{2-} mass concentration decreased obviously on August 1, and then remained at approximately 200 ng m^{-3} most of the time.

The WSIs data that were collected hourly during the whole observation period and the SF and NSF periods were statistically analyzed, and a summary of the average WSIs concentrations during these different periods is presented in Table 1. The average WSIs mass concentrations during the SF, NSF and whole period were in the following order: nss-SO_4^{2-} > Na^+ > Cl^- > Mg^{2+} > ss-SO_4^{2-} > K^+ > Ca^{2+} > MSA^- > NO_3^-. Fig. S1 lists the mean contributions of each analyzed ion to the total ion mass concentration during the SF, NSF and whole period. The first three ions accounted for over 80% of the total ion mass concentration. The nss-SO_4^{2-} concentrations during the observation period ranged from approximately 100 ng m^{-3} to 400 ng m^{-3}, with a mean of 187.01 ng m^{-3}. The Na^+ concentrations were in the range from 5.65 to 420.26 ng m^{-3} with a mean of 99.03 ng m^{-3}. The Cl^- concentrations varied from 9.94 ng m^{-3} to 296.81 ng m^{-3} with a mean of 60.55 ng m^{-3}. Table 2 lists a comparison of our measurements to those from previous studies over the Arctic Ocean and subarctic western North Pacific Ocean. Results of our study were similar to the previous studies (Jung et al., 2013; Yu et al., 2020; Mukherjee et al., 2021) in some places: sea salt ions (contained Na^+, Cl^-, Mg^{2+}, ss-SO_4^{2-}, K^+, and Ca^{2+}) were the dominant ions, and then followed by nss-SO_4^{2-}, while concentrations of NO_3^- and MSA^- were much lower. Higher concentrations over the western north Pacific Ocean than those obtained in this study may be due to different study areas, that large area of open sea without sea ice may be originated more sea salts ions; and air masses originated from the Asian continent and the Kamchatka Peninsula indicating that the higher concentrations of ions may also affected by anthropogenic and crustal sources as well as the eruptions of two volcanoes (Jung et al.,

Table 1
Statistical analyzed values of WSIs in aerosol particles during the observation period.

	WSIs in aerosol particles/ng.m^{-3}								
	Na^+	K^+	Mg^{2+}	Ca^{2+}	MSA^-	Cl^-	NO_3^-	ss-SO_4^{2-}	nss-SO_4^{2-}
Sea fog periods									
Mean	**72.41**	**8.42**	**23.34**	**4.33**	**1.98**	**43.83**	**1.74**	**17.43**	**225.30**
SD	76.03	12.94	9.83	9.14	1.42	40.89	1.74	19.04	53.50
Min	5.65	1.11	11.12	0.06	0.19	10.49	0.06	0.00	147.30
Med	39.14	4.68	20.92	2.85	1.43	24.76	1.19	8.95	212.66
Max	335.54	84.52	55.70	72.03	5.12	207.24	7.46	83.89	424.14
N	69	46	66	63	66	70	42	66	66
Non sea fog periods									
Mean	**107.54**	**9.51**	**30.76**	**8.63**	**1.33**	**65.93**	**1.11**	**27.13**	**174.85**
SD	97.03	16.67	18.81	11.08	1.05	56.21	1.12	24.53	30.89
Min	6.51	0.24	9.18	0.36	0.02	9.94	0.01	1.63	109.38
Med	77.77	5.30	21.81	5.74	1.12	43.75	0.84	19.83	173.8
Max	420.26	178.91	96.96	98.54	5.42	296.81	5.97	105.06	254.18
N	216	162	209	191	201	218	87	210	211
Whole periods									
Mean	**99.03**	**9.27**	**28.98**	**7.56**	**1.49**	**60.55**	**1.29**	**24.67**	**187.01**
SD	93.49	15.90	17.36	10.78	1.19	53.67	1.35	23.65	43.16
Min	5.65	0.24	9.18	0.06	0.02	9.94	0.00	0.00	109.38
Med	65.06	5.10	21.45	4.80	1.16	37.62	0.87	16.12	180.70
Max	420.26	178.91	96.96	98.54	5.42	296.81	7.46	105.06	424.14
N	285	208	275	254	267	288	129	276	277

Table 2
Comparison with other studies.

Study area (observation time)	Average WSIs in aerosol particles/ng.m^{-3}								
	Na^+	K^+	Mg^{2+}	Ca^{2+}	Cl^-	MSA^-	NO_3^-	nss-SO_4^{2-}	References
Arctic Ocean (August 1 to 12, 2017)	99.03	9.27	28.98	7.56	60.55	1.49	1.29	187.01	This study
Arctic Ocean (July 29 to September 7, 2018)	930	100	20	20	470	20	40	180*^{a}	Yu et al. (2020)
Arctic Ocean (August 10 to October 12, 2015)	3600*^{1}					72	120	190	Mukherjee et al. (2021)
	370*^{2}					3.6	2.9	21	
	6400*^{3}					1.4	22	35	
Western North Pacific Ocean (July 29–August 19, 2008)	759	23.01	70.8	36	994	59.58	155	864	Jung et al. (2013)

Note: Mukherjee et al. (2021) divided their study period into three segment according to the air masses: *^{1}, *^{2} and *^{3} represent the segment 1, 2 and 3; the values represent the concentrations of all sea salt ions. *^{a} the data were the concentration of SO_4^{2-}.

2013). Higher concentrations of sea salt ions, NO_3^- and MSA^- over the Arctic Ocean (Yu et al., 2020) than our results may be caused by their longer sampling period. In our study, the sampling period was shorter and most of the sampling period were with sea ice regions, besides the removal of sea fog events may be also one of the influence factors result in the lower concentrations. Average WSIs concentration levels in our study were comparable to the segment 2 study results by Mukherjee et al. (2021) over the Arctic Ocean, which were mainly influenced by the polar marine air and sea-ice coverage may reduce the production of sea-salt ions.

In this study, the average mass concentrations of Na^+, K^+, Mg^{2+}, Ca^{2+}, MSA^-, Cl^-, NO_3^-, ss-SO_4^{2-} and nss-SO_4^{2-} during the sea fog processes, were 72.41 ng m^{-3}, 8.42 ng m^{-3}, 23.34 ng m^{-3}, 4.33 ng m^{-3}, 1.98 ng m^{-3}, 43.83 ng m^{-3}, 1.74 ng m^{-3}, 17.43 ng m^{-3} and 225.30 ng m^{-3}, respectively, while during the non-sea fog processes, they were 107.54 ng m^{-3}, 9.51 ng m^{-3}, 30.76 ng m^{-3}, 8.63 ng m^{-3}, 1.33 ng m^{-3}, 65.93 ng m^{-3}, 1.11 ng m^{-3}, 27.13 ng m^{-3} and 174.85 ng m^{-3}, respectively. The average mass concentrations of Na^+, K^+, Mg^{2+}, Ca^{2+}, Cl^- and ss-SO_4^{2-} during the SF period were obviously lower than those during the NSF period, while nss-SO_4^{2-} concentrations during the SF processes were much higher than those in the NSF period; MSA^- and NO_3^- levels were slightly higher than those in the NSF period. The relative contribution of ions during SF and NSF were slightly different (in Fig. S1), it can be seen that the average contributions of Na^+, K^+, Mg^{2+}, Ca^{2+}, MSA^-, Cl^-, NO_3^-, ss-SO_4^{2-} and nss-SO_4^{2-} during SF were 18.2%, 2.1%, 5.9%, 1.1%, 0.5%, 11%, 0.4%, 4.4% and 56.5% respectively; while during NSF were 25.2%, 2.2%, 7.2%, 2.0%, 0.3%, 15.4%, 0.3%, 6.4% and 41%. The differences in ion concentrations and contribution ratios during SF and NSF may cause by many factors. One possible reason is that partial ions in aerosol particles may serve as fog condensation nuclei easily, thus the chemical ions entering into the fog droplets or fog waters while some chemical components are not easy act as fog condensation nuclei and stay in aerosol particles. Besides, the removal of fog droplets during sea fog processes may be another reason for the change of chemical composition of aerosol during SF and NSF. Detailed discussions are listed in section 3.3.

3.2. Spatial distributions of sea fogs and aerosol WSIs over the Arctic Ocean

Spatial distributions of sea fog processes and aerosol WSIs over the Arctic Ocean are shown in Fig. 3. According to the description in Section 2.1, SF1 occurred over a zone without sea ice. After SF1, the ship sailed among the ice floes, and before SF2, the ship entered an area with dense floating ice and a sea ice density greater than 70%. According to Fig. 3a, SF1 occurred over the Chukchi Shelf near the coastal area, while SF2 and SF3 occurred mainly over the Arctic Ocean basin where there was dense floating ice. Na^+, nss-SO_4^{2-} and MSA^- exhibited obviously different spatial distributions (Fig. 3b, c and d), which may be correlated to both the emissions/transport inputs and removal processes. Na^+ first gradually decreased from the Chukchi Shelf to the Arctic Ocean during the Expedition (Fig. 3b) and then slightly increased at the beginnings of SF2 and SF3; the highest Na^+ value was observed at 81.5°N and 160°E, which coincided with strong wind. Except for the above area, the concentrations of Na^+ seemed decreased significantly. Removal effect during the SF period may be the primary factor resulted in the decrease,

while another reason may be their decreased emissions caused by the sea-ice coverage after entering into the dense floating ice area. May et al. (2016) reported that the sea-salt aerosol formation was highly dependent on wind speed and sea-ice coverage; their study showed that about 2 times higher sea-salt concentrations were measured over open water than that covered with sea-ice area. Mukherjee et al. (2021) also found that sea-ice coverage reduced the production of sea-salt aerosols. The nss-SO_4^{2-} concentrations gradually decreased as the route continued towards the north (Fig. 3c). the highest (and the relatively high) nss-SO_4^{2-} concentrations (above 250 ng m^{-3}) were recorded during SF1, which occurred over the Chukchi Shelf near the coastal area, and gradually decreased when the ship left the coastal area and sailed into the Arctic Ocean. Although MSA^- concentrations were much lower than those of sea salt ions and nss-SO_4^{2-}, they exhibited obviously different spatial distributions (Fig. 3d). The highest (and the relatively high) MSA^- concentrations (over 4 ng m^{-3}) were observed mainly over the Chukchi Shelf, and sporadically high values were measured near 85°N and 120°E; most of the MSA^- concentrations were less than 3 ng m^{-3} in other areas. Previous studies (Springer et al., 1996; Li et al., 2020; Liu et al., 2011) reported that diatoms were the primary source of the Chukchi Shelf; the Chukchi Sea Shelf area had high amounts of diatoms and an extremely high rate of accumulation of labile organic matter. MSA and partial nss-SO_4^{2-} are the primary oxidation products of DMS, which is released by phytoplankton such as diatoms. Thus, higher concentrations of nss-SO_4^{2-} and MSA^- above the Chukchi Shelf may be caused by the release of these substances by diatoms. Higher MSA^- values near 85°N and 120°E (a region of dense sea ice) may be caused by long-range transport of MSA^- from other regions. In addition to the oxidation of DMS, there are several other sources of nss-SO_4^{2-}, including volcanic and anthropogenic inputs that may form from SO_2. According to the backward trajectory results (Fig. 4), the air masses affecting SF1 over the Chukchi Shelf area originated mainly in the continental shelf area, while the air masses affecting SF2 and SF3 were mainly from the marine area. The higher nss-SO_4^{2-} level over the Chukchi Shelf area may also be influenced by anthropogenic inputs; with the air masses changing to those marine origin, the anthropogenic inputs decreased, and the nss-SO_4^{2-} concentrations decreased and became lower than those over the Chukchi Shelf. Similar spatial variations of NO_3^- can also be found during this region.

3.3. Changes in aerosol WSIs during different sea fog processes

To evaluate the differences between sea fog and non-sea fog processes, the effects of sea fog processes on the chemical characteristics of TSPs and WSIs during SF and NSF periods were calculated by independent samples tests. The results are listed with the F-statistic and significance values in Table S3. A significance value of $p < 0.05$ was the threshold for statistically significant differences between dependent variables. Concentrations of Na^+, Cl^-, Mg^{2+}, MSA^-, ss-SO_4^{2} and nss-SO_4^{2-} exhibited statistically significant differences between sea fog and non-sea fog periods, whereas there were no statistically significant differences for NO_3^-, K^+ and Ca^{2+}. This result suggests that the sea fog processes obviously influenced the Na^+, Cl^-, Mg^{2+}, MSA^-, ss-SO_4^{2} and nss-SO_4^{2-} ions and may have had less impact on the NO_3^-, K^+ and Ca^{2+} ions. Changes in the concentrations of Na^+, Cl^-, Mg^{2+}, MSA^-, ss-SO_4^{2} and nss-SO_4^{2-} during the 3 sea fog events are discussed in detail, including the occurrence and development of the sea fog periods and subsequent conditions.

Fig. 5 shows the variations in the concentrations of Na^+, Cl^-, Mg^{2+}, MSA^-, ss-SO_4^{2} and nss-SO_4^{2-} during the 3 sea fog periods. Before the occurrence of sea fog, the mass concentrations of sea salt ions, such as Na^+, Cl^-, Mg^{2+} and ss-SO_4^{2-}, first increased obviously; at the beginning of the occurrence of sea fog events, concentrations of Na^+, Cl^-, Mg^{2+} and ss-SO_4^{2} decreased significantly in a short time and then remained at a low throughout and after the sea fog events. These variations may correlate with the aerosol nucleation mechanism and the formation and development of the sea fog processes. A previous study reported that fog occurrence usually correlated with strong winds (Gultepe et al., 2007). It can be found that before SF processes, wind speeds were approximately 9 m s^{-1} in SF1, while wind speeds increased obviously, even from approximately 3 m s^{-1} to more than 9 m s^{-1}, in SF2 and SF3 (Fig. S2). As high wind speed over the ocean surface usually caused more bursting bubble or droplet formation (Exton et al., 2010; Yu et al., 2020), increasing sea salt ion concentrations before SF processes may be primarily due to higher or increasing wind speed. Chen et al. (2019) reported that the advection fogs (SF1, SF2 and SF3) over the Arctic Ocean ice floe regions were formed by the cooling and condensation of the warm southerly humid air mass on the surface of the cold ocean or sea ice. A similar phenomenon also frequently occurs in the North Pacific Ocean regions in the summertime. Sasakawa et al. (2003) reported that when warm and wet air masses from the low and middle latitudes of the North Pacific Ocean pass over the cold sea surface of the northern North Pacific Ocean, they cools to a saturation temperature sufficiently low for the formation of sea fog. It has been proposed that marine particles can lead and provide material for both nucleation and larger particle formation (Leck and Bigg, 1999; Lange et al., 2019). Due to the curvature effect, coarse particles are more likely to serve as fog condensation nuclei and can be removed effectively by sea-fog (Sasakawa et al., 2003; Fahey et al., 2005; Jung et al., 2013). Above the ocean surface, coarse particles such as sea-salt aerosol particles, rather than the fine particles such as NO_3^- and nss-SO_4^{2-}, usually act predominantly as condensation nuclei for sea fog droplets (Sasakawa and Uematsu, 2002; Sasakawa et al., 2003). Increased concentrations of Na^+, Cl^-, Mg^{2+} and ss-SO_4^{2} ions before SF events may have included some larger particles, which

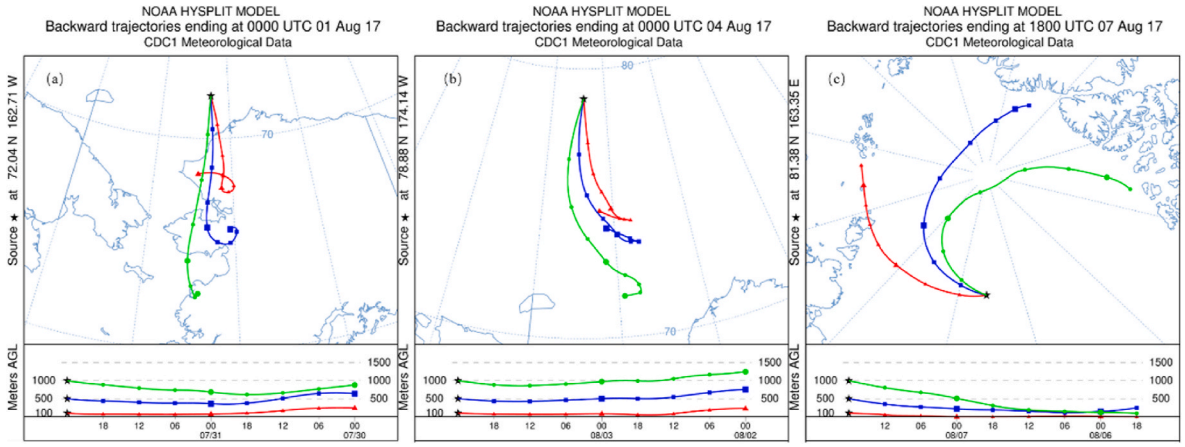

Fig. 4. Backward air mass trajectories arriving at the Arctic Ocean: Trajectories terminated at the beginning of SF1 (a), SF2 (b) and SF3 (c).

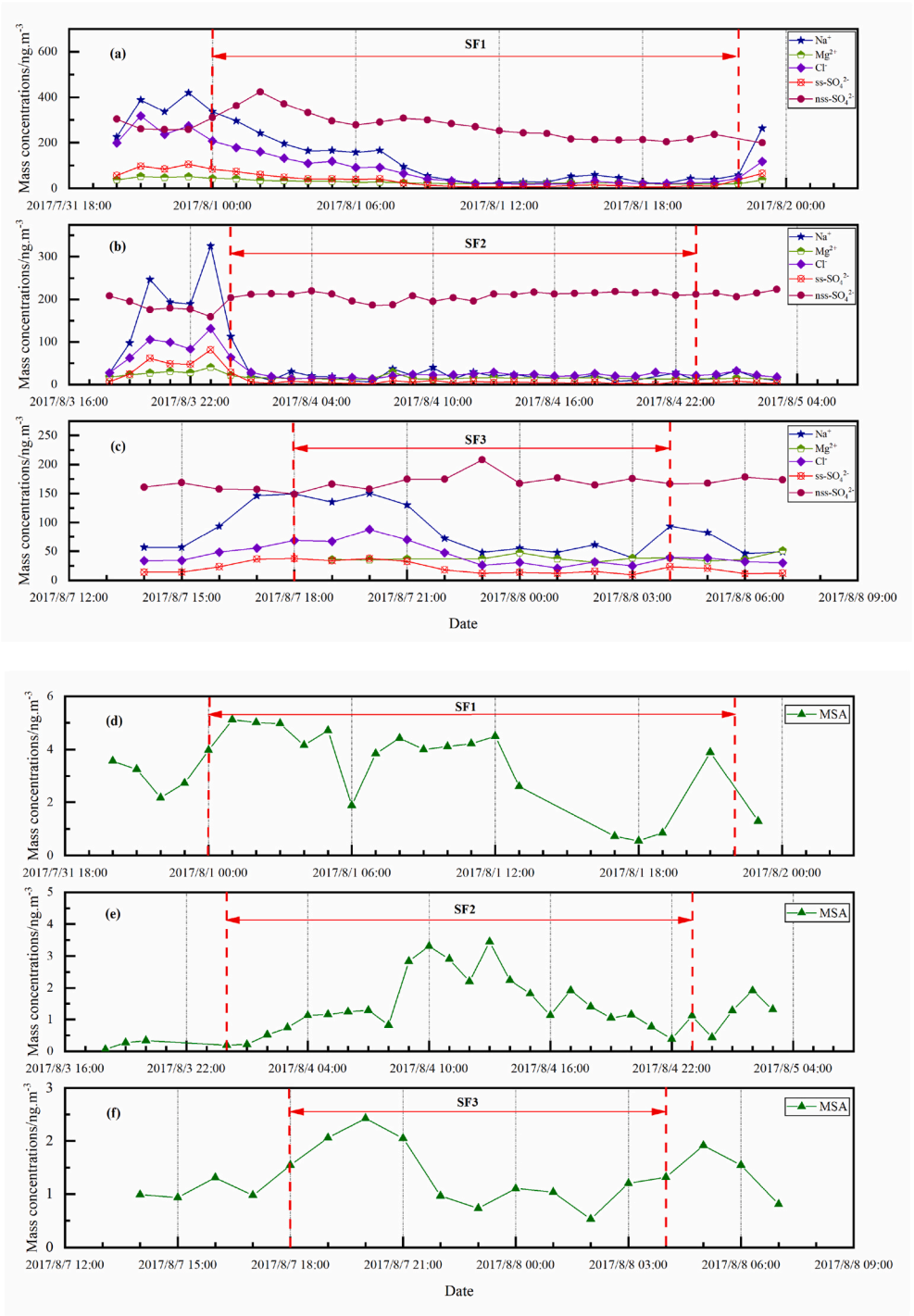

Fig. 5. Mass concentrations of Na^+, Cl^-, Mg^{2+}, ss-SO_4^{2} and nss-SO_4^{2-} during SF1 (a), SF2 (b) and SF3 (c); and MSA^- during SF1 (d), SF2 (e) and SF3 (f).

were more likely to become fog condensation nuclei and were prone to form large fog droplets. In addition to their large size, sea salt particles were hydrophilic. When the mass concentrations of hydrophilic sea salt ions in aerosol particles reached a sufficiently high level, under the influence of continuous supersaturated water vapor, these hydrophilic ionic particles may develop into fog condensation nuclei, forming sea fog. After fog formation, aerosol particles and gases can enter fog droplets by Brownian motion or diffusion to participate in chemical reactions (Yue et al., 2014). Thus, with the formation and development of sea fogs, the concentrations of hydrophilic sea salt ions in the fog droplets increased, and the corresponding ion concentrations in the aerosol particles decreased significantly. In other words, the sea fog process can result in a decrease in the concentration of sea salt ions, such as Na^+, Cl^-, Mg^{2+}, and ss-SO_4^{2-}, in the atmospheric particles, proving the behavior of the condensation nuclei of sea fog droplets and the removal or deposition effect of sea fog.

During SF1 (Fig. 5a), the mass concentrations of these ions decreased during the first 9 h, and then remained at much lower concentrations until the end of the sea fog event. Concentrations during SF2 (Fig. 5b) and SF3 (Fig. 5c) were lower at 2 h and 6 h, respectively. One reason for the differences between SF1 vs. SF2 and SF3 may be correlated with the sea ice cover; it is possible that during SF2 and SF3, Na^+, Cl^-, Mg^{2+}, ss-SO_4^{2-} were little emitted from the sea surface due to sea ice cover. During SF1, except for fog removal or deposition, higher wind speeds (as

shown in Fig. S2) still affected sea salt particle formation; thus, in the SF1 process, the sea salt ion decrease lasted a slightly longer time. Slightly longer persistence during SF3 may also correlate with much higher wind speed (as shown in Fig. S2) and long-range high latitude transport input (Fig. 4c). A similar situation was found by (Sasakawa et al., 2003); since sea salt was continuously supplied from the sea surface, the Na^+ concentration did not decrease. However, regardless of whether the decrease lasted for a long time, the concentrations of Na^+, Cl^-, Mg^{2+} and ss-SO_4^{2-} decreased to their minimum values in the second half of the sea fog process and then remained at low concentrations until the end of the sea fog event. After the sea fog processes, the sea salt ion concentrations usually remained at low concentrations for several hours (as shown in Fig. 5b and c), except for another sea fog formation event which was influenced by the high wind speed processes or the long-range transport inputs (as shown in Fig. 5a).

In contrast to Na^+, Cl^-, Mg^{2+} and ss-SO_4^{2-}, nss-SO_4^{2-} showed no obvious decrease during these sea fog processes. The nss-SO_4^{2-} concentrations increased before SF1 occurred, continued to increase with the beginning of the sea fog event, reached a maximum value, then decreased slowly, and then remained above 200 ng m^{-3} until the end of SF1. During SF2, the nss-SO_4^{2-} concentrations first slightly decreased and then increased before the occurrence of SF2 and were maintained at approximately 200 ng m^{-3} during the whole SF process, from the beginning to the end and even after the end of the SF2 process. During SF3, the nss-SO_4^{2-} concentrations were almost the same before occurrence, during development and after the end of the event. The reasons for that behavior of nss-SO_4^{2-} may be caused by their different size distribution and solubility. Mukherjee et al. (2021) reported that nss-SO_4^{2-} over the Arctic Ocean predominately in fine-mode particle. Fine secondary nss-SO_4^{2-} particles are not easy to nucleate and removed by the SF processes. Previous study by Sasakawa et al. (2003) also pointed out that sea salt particles served as condensation nuclei of sea fog droplets more efficiently than NH_4^+ and nss-SO_4^{2-} particles, while Yue et al. (2012) found that Na^+, Cl^- sea salt ions, rather than nss-SO_4^{2-} secondary ions, were the main ions in sea fog and fog water and further verified the contribution of sea salt aerosols to sea fog condensation nuclei. Aikawa et al. (2007) reported that ion species such as Na^+, Ca^{2+}, Cl^- and NO_3^- were easily and effectively scavenged by fog water, while sulfur species such as SO_4^{2-} (p) and SO_2 (g) could not be easily and effectively scavenged by fog water because of the poor solubility of SO_2 (g). In addition to the above reasons, nss-SO_4^{2-} during these three SF processes, may also include some aged and fine particles that formed through secondary transformations (the conversion of SO_2/DMS to nss-SO_4^{2-}) and underwent long transport processes and came with warm southerly humid air masses. Thus, unlike sea salt ions, the mass concentrations of nss-SO_4^{2-} did not decrease but were maintained at their higher values during the SF processes; alternatively, nss-SO_4^{2-} particles may not easily nucleate and are removed during the sea fog processes.

Sasakawa and Uematsu (2005) reported that sea fog scavenges MSA more effectively than rain. In this study, the mass concentrations of MSA^- were much lower than those of Na^+, Cl^-, Mg^{2+}, ss-SO_4^{2-}, and nss-SO_4^{2-}. Lower concentrations suggested a small biogenic contribution during this period. Fig. 5d, e and f show that MSA^- underwent different variations during the 3 SF processes. It has been reported that MSA can participate in the nucleation and growth of aerosol particles, thereby affecting clouds and climate (Charlson et al., 1987; Lovelock et al., 1972). However, MSA^- did not show an obvious decrease during SF1 and SF2, although similarly decreasing variation can be found in SF3. MSA^- concentration first increased before SF events and for 2 h after SF began and then decreased with variations similar to those of Na^+ ions. Different characteristics of MSA^- during SF processes may be mainly caused by its biogenic source, which is different from generation processes such as those that involve sea salt ions and secondary nss-SO_4^{2-}. A similar change trend to sea salt ions in SF3 may be due to MSA^- adsorption, because MSA is easily adsorbed on sea salt particles during its generation processes (Yan et al., 2020b). Because it is favorable for alkaline sea salt particles to absorb acidic atmospheric gases, promoting the formation of acidic compounds on sea salt particles, MSA (an acidic species) is easily absorbed by sea salt particles to form particulate MSA. Additionally, the presence of halogen radicals on sea salt particle surfaces enhances the oxidative reactive uptake of DMS on those particles to form particulate MSA (Laskin et al., 2003; Read et al., 2008). High uptake rates of MSA-Na and MSA-Mg particles have been observed in the polynya regions of the Ross Sea, Antarctica (Yan et al., 2020b). Therefore, MSA may combine with sea salts, which nucleate particles that are removed by sea fog.

3.4. Interactions between aerosols and sea fog in the sea ice regions of the Arctic Ocean

Previous studies have been carried out on the meteorological and physical processes of sea fog (Wang et al., 1985; Gilson et al., 2018; Yang and Gao, 2020). They have shown that the formation of sea fog requires two processes: condensation of water vapor and accumulation of water droplets at low altitude. During these two processes, two conditions must be met. First, the water droplets must be suspended in the offshore surface layer to reduce horizontal visibility. Second, there must be condensation nuclei, such as aerosol dust particles, present during condensation. During the observation period, the RH was almost 100% most of the time (as shown in Fig. 2), and the water vapors were saturated or nearly saturated (as shown in Fig. S3). The air temperature must drop below the dew point as a necessary condition for water vapor condensation, and the difference between these two temperatures indicates the degree of saturation of water vapor in the air. Except for several hours on August 5, 6, 7 and 9, most of the air temperatures were the same as the dew point temperature, and the air temperature-dew point difference was 0 °C (Fig. S3), indicating that the water vapor in the air was saturated. This provided favorable conditions for the formation of sea fog. However, sea fog was not formed at all the times when the water vapor was saturated because of the second condition mentioned above, i.e., condensation nuclei must be present.

The correlation between WSIs and meteorological data during the SF and NSF periods (Table 3) showed that sea slat ions, such as Na^+, Cl^-, Mg^{2+} and ss-SO_4^{2-} exhibited statistically significant positive correlation coefficients with wind speed. This confirmed that continually strong winds may have produced many coarse hydrophilic sea salt particles such as Na^+, Cl^-, Mg^{2+} and ss-SO_4^{2-} particles, which were likely to serve as fog condensation nuclei, forming and generating sea fog. Some differences were also found during the SF and NSF periods (Table 3). Fig. 6 showed the wind direction and wind speed frequencies, and correlation between sea salt ions with wind speed and wind direction during the SF period and NSF period. During the NSF period, the wind came mainly from the northwest, west and southwest with high speeds (as shown in Fig. 6b). Under these conditions, Na^+, Cl^-, Mg^{2+} and ss-SO_4^{2-} sea salt ions seemed increased with western/northwestern winds from the ocean and higher wind speeds (as shown in Fig. 6d). In addition, during the NSF periods, sea salt ions, such as Na^+, Cl^-, Mg^{2+} and ss-SO_4^{2-}, exhibited statistically significant positive correlations only with wind speed, while nss-SO_4^{2-} showed negative correlation coefficients, suggesting that during this period, wind direction and wind speed may be important factors influencing the WSIs. During SF periods, the winds were mainly from the southeast, south and southwest (as shown in Fig. 6a), and sea salt ions, such as Na^+, Mg^{2+} and ss-SO_4^{2-}, exhibited a significant positive correlation with only wind speed. From Fig. 6c, it can be seen that higher concentrations of sea salts were found at higher wind speeds with southeast and northwest wind direction, which different from the situation during NSF periods.t In addition to this, unlike the NSF periods, during the SF events, Na^+, Cl^- and ss-SO_4^{2-} exhibited significant positive correlation coefficients with air temperature (T-air), sea surface temperature (T-sw) and dew point temperature (Td); Mg^{2+} and Ca^{2+} exhibited significant positive correlation coefficients with T-sw. These results suggested that over the sea ice regions of the Arctic Ocean, the

Table 3
Correlation between ions and meteorological data.

Meteorological data Ions	T-air	T-sw	Td	WS	RH	Vis
Sea fog period						
Na^+	**0.477****	**0.489****	**0.474****	**0.311****	−0.212	0.191
K^+	−0.215	−0.137	−0.219	**0.380****	−0.114	0.227
Mg^{2+}	0.233	**0.424****	0.236	**0.427****	**−0.349****	0.240
Ca^{2+}	−0.092	**0.464****	−0.093	0.261*	−0.124	0.127
MSA^-	**0.746****	0.143	**0.743****	0.087	0.141	−0.305*
Cl^-	**0.618****	**0.549****	**0.615****	0.270*	−0.079	0.041
NO_3^-	0.058	−0.094	0.056	−0.025	0.035	0.308*
ss-SO_4^{2-}	**0.478****	**0.489****	**0.475****	**0.323****	−0.211	0.197
nss-SO_4^{2-}	**0.660****	0.268	**0.662****	−0.170	0.227	−0.071
Non sea fog period						
	T-air	**T-sw**	**Td**	**WS**	**RH**	**Vis**
Na^+	−0.024	0.215	−0.056	**0.605****	−0.078	0.100
K^+	−0.064	−0.013	−0.078	0.115	−0.071	0.136
Mg^{2+}	−0.056	0.030	−0.084	**0.557****	−0.098	0.098
Ca^{2+}	0.042	−0.176	0.041	0.075	0.004	0.032
MSA^-	**0.203****	−0.194	**0.222****	**0.304****	0.100	**0.203****
Cl^-	−0.042	0.112	−0.058	**0.586****	−0.047	0.146*
NO_3^-	0.183	−0.053	0.166	0.108	−0.034	−0.172
ss-SO_4^{2-}	−0.027	0.223	−0.06	**0.605****	−0.081	0.099
nss-SO_4^{2-}	0.036	0.085	0.054	**−0.318****	0.053	−0.060

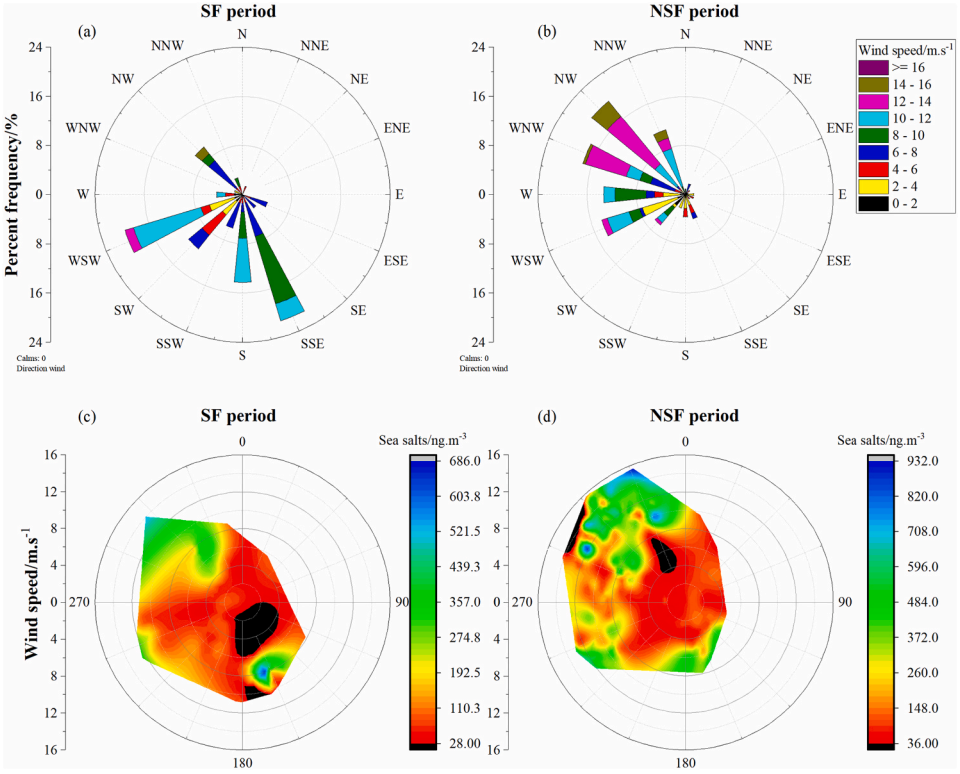

Fig. 6. Wind direction and wind speed frequencies during the a) SF and b) NSF period; and the correlation between sea salt ions with wind speed and wind direction during the s) SF and d) NSF period.

origination of sea salt ions increased with the air temperature dew point temperature and sea surface temperature increase. Previous studies reported that during the daytime, the oxidation of DMS occurred mainly through two reactions: one addition reaction with OH produced dimethylsulfoixide (DMSO) and MSA, and the other abstraction reaction with OH produced mainly SO_2 and ultimately sulfuric acid (H_2SO_4); both reactions have a significant dependence on temperature (Hynes et al., 1986; Barnes et al., 2006; Albu et al., 2006; Castebrunet et al., 2009); the former reaction is favored at −42 °C, and the other reaction is favored at approximately 17 °C. As shown in Fig. 2 and Fig. S3, after the appearance of ice floes on August 2 at 00:00, most of the air temperature measurements were below 0 °C. Significant positive correlation coefficients between MSA^- and T-air, nss-SO_4^{2-} and T-air-like sea salt ions, indicate that during this period, MSA^- and nss-SO_4^{2-} increased with the air temperature.

Chen et al. (2021) reported that with high RH, sea salt particles can uptake water or be activated to form cloud droplets (>critical supersaturation ratio) that enhance aqueous phase reactions. The significant water content can promote sea salt particles to undergo further chemical reactions. In this study, sea salt ions, such as Na^+, Cl^-, Mg^{2+} and

ss-SO_4^{2-}, were likely to serve as fog condensation nuclei and then be scavenged by fog droplets. To estimate the fog scavenging effects on aerosol particles, the scavenging ratio of a WSI was calculated by Si = (1-Ci-b/Ci-e)*100 according to the previous studies (Hallberg and Orgen, 1992; Gilardoni et al., 2014; Heintzenberg et al., 2016), where Si represent the scavenging ratio of ion i (one of the WSIs), Ci-b represents the mass concentration of ion i 1 h before sea fog generation, and Ci-e represents the mass concentrations of ion i at the final hour during the sea fog processes. Fig. 7 shows that the scavenging ratios of Na^+, Cl^-, and ss-SO_4^{2-} during SF1 and SF2 were more than 80%, while those during SF3 were approximately 30%. During SF1 and SF2, the scavenging ratios of Mg^{2+} and Ca^{2+} were more than 60%. During SF1, the scavenging ratios of some secondary ions, such as nss-SO_4^{2-}, was less than 10%, and the scavenging ratio for MSA^- was approximately 50%. However, during SF2 and SF3, the mass concentrations of these two ions did not decrease but increased before sea fog generation; the negative values are not listed in Fig. 7. A similar situation was found for NO_3^- during SF2 and SF3, and some data collected during SF1 are missing; thus, NO_3^- is not listed in Fig. 7. Chen et al. (2021) reported that larger particles have higher fog scavenging removal efficiencies, while smaller particles continue to grow through gas-to-aqueous solution partitioning. As discussed in Section 3.3, the higher scavenging ratios of sea salt ions may be due to their larger size and the curvature effect; coarse particles are more likely to serve as fog condensation nuclei and can be removed effectively by sea-fog (Sasakawa et al., 2003; Fahey et al., 2005), while secondary smaller particles such as NO_3^- and nss-SO_4^{2-} may continue to grow during sea fog processes; thus, their scavenge ratios were small and even increased. The results were different from those of the previous study by Sasakawa et al. (2003). They found that during a sea fog process over the northwestern North Pacific Ocean, concentrations of nss-SO_4^{2-} and NO_3^-, which originate from anthropogenic activity, decreased as sea fog formed, while as sea salt was continuously supplied from the sea surface, the Na^+ concentration did not decrease (Sasakawa et al., 2003). The differences may be caused by several reasons. First, the sea fog processes were complicated, and although the sea fog had a similar pattern, there were still many different situations. Thus, the fog condensation and scavenging ratio were not the same. Second, different ocean areas may have different characteristics. In this study, MSA^-, nss-SO_4^{2-} and NO_3^- did not seem to decrease obviously, while sea salt ions were scavenged suddenly with sea fog formation. The variations in sea salt ion concentrations over time from sea fog formation during the three sea fog processes are shown in Fig. 8. The rates of decrease WSIs were calculated as described by Sasakawa et al. (2003). The decrease rates of Na^+, Cl^-, and ss-SO_4^{2-} were 0.19, 0.19 and 0.18 during SF1 and 3.83, 1.95, and 3.52 during SF2, respectively, but fitting the from SF3was unsuccessful. The difference in the decrease rate between Na^+ and Cl^-, may be caused by the Cl depletion, that NaCl may reacts with other ions to form HCl, resulting in a loss of Cl in the particles (Yao et al., 2003; Yu et al., 2021). Condensation may be the primary factor leading to the reduction of sea salt ions during the sea fog periods, while other factors like the presence of dense sea ice and long-range transport input may also affect the decreasing rate. Except for the condensation, differences between these three sea fog processes and the higher rate of decrease during SF2 may be due to spatial variations and the presence of dense sea ice. From the relative humidity profile in the open sea area, it can be seen that the entire boundary layer atmosphere was saturated, and the low visibility caused by the sea fog did not change much with altitude, while in the region of dense ice floes, there was a strong inverse moisture layer at the bottom of the boundary layer, indicating that the sea fog was thin close to the ice and snow surface, and it increased rapidly in thickness as the altitude increased. This is because sea ice isolates water vapor transport at the sea-air interface, and the water vapor in the boundary layer comes mainly from advection transport (Chen et al., 2019). SF1 occurred over the zone without sea ice, while SF2 and SF3 occurred over the dense sea ice regions. In addition to isolating the water vapor transport at the sea-air interface, dense sea ice separates the exchange at the sea-air interface; thus, sea salts may not be supplied continuously from the sea surface over ice floe areas, and the decreasing rate during SF2 seemed higher than that during SF1. Different characteristics during SF3 may be also influenced by its

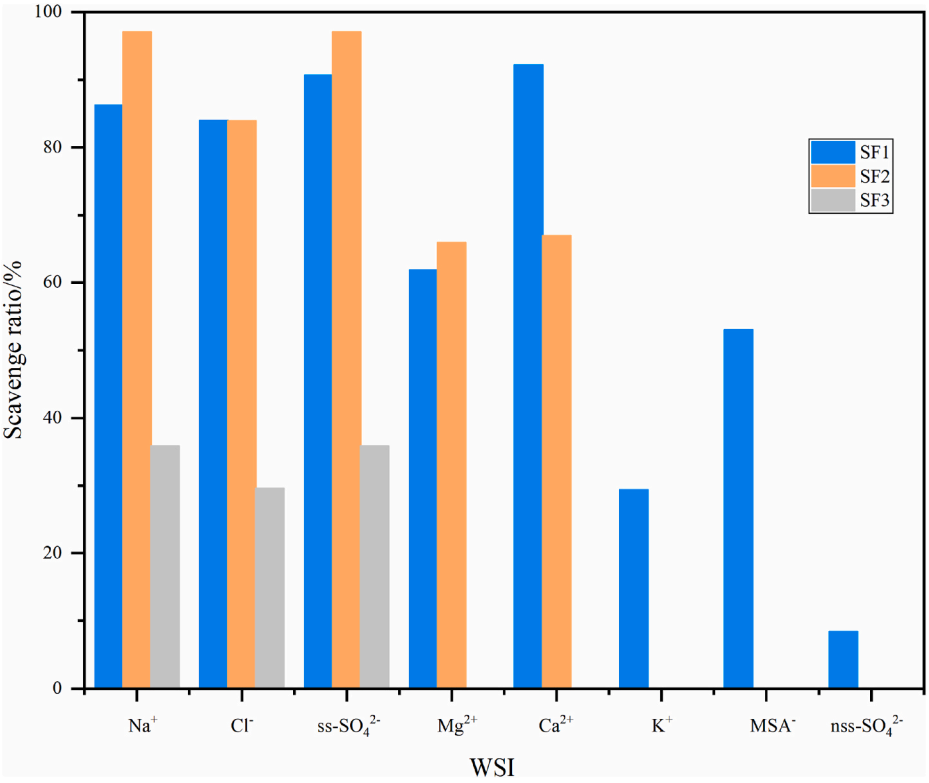

Fig. 7. Scavenge ratio of WSIs during three sea fog processes.

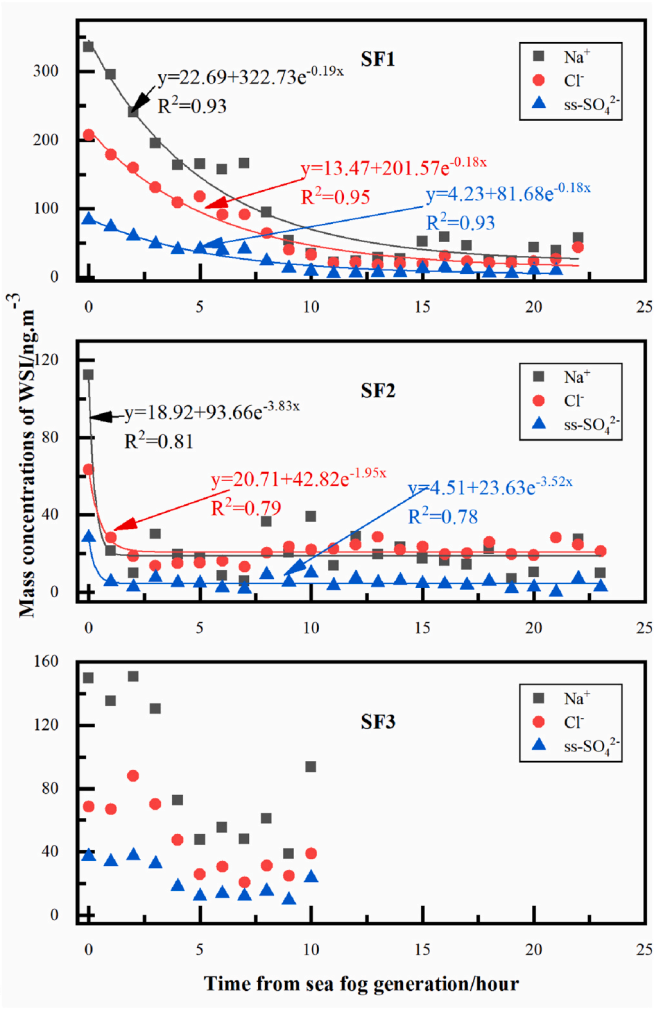

Fig. 8. Variation of sea salt ions concentrations against time from sea fog generation during three sea fog processes.

different originating air masses, and continuous supply from the western ocean area may input some sea salts 2 h after sea fog was generated. In addition, higher relative humidity in the planetary boundary layer (PBL), together with the direct effect of aerosols, caused stronger wet deposition that greatly exceeded their production by aqueous phase chemistry (Jung et al., 2021). During SF3, there was a strong inverse moisture layer at the bottom of the boundary layer, indicating that the sea fog was thinner close to the sea ice surface, and it increased rapidly in thickness as the altitude increased. The unstable stratification in the lower part of the boundary layer and the instability of the convection induced by wind speed shear caused the air to rise and condense, which further increased the thickness and maintained the sea fog in the upper part of the boundary layer (Chen et al., 2019).

4. Conclusions

Sea fog and aerosol chemistry were studied during the 8th Chinese National Arctic Research Expedition (CHINARE). We used the results of sea fog characterizations by Chen et al. (2019) to study the interactions between sea fog processes and aerosol chemistry. High-resolution time-resolved in situ online measurements of water-soluble ions in aerosols were performed over the Arctic Ocean ice floe regions from August 1 to 12, 2017, when sea fog was frequently observed. The results showed statistically significant differences for concentrations of Na^+, Cl^-, Mg^{2+}, MSA^-, ss-SO_4^{2} and nss-SO_4^{2-} ions between sea fog and non-sea fog processes, whereas there were no statistically significant differences for NO_3^-, K^+ and Ca^{2+} had. This result suggests that the sea fog processes obviously influenced Na^+, Cl^-, Mg^{2+}, MSA^-, ss-SO_4^{2} and nss-SO_4^{2-} ions and may have had little or no impact on NO_3^-, K^+ and Ca^{2+} ions. The average mass concentrations of Na^+, K^+, Mg^{2+}, Ca^{2+}, Cl^- and ss-SO_4^{2-} during the sea fog processes were obviously lower than those during the non-sea fog periods, while nss-SO_4^{2-} concentrations during sea fog processes were higher than those in the non-sea fog periods. This may be caused by the removal of those sea salt ions by sea fog. Although the mass concentrations of sea salt ions, such as Na^+, Cl^-, Mg^{2+} and ss-SO_4^{2-}, obviously increased before the occurrence of sea fog and then continued to increase with the beginning of sea fog formation, Na^+, Cl^-, Mg^{2+} and ss-SO_4^{2} decreased significantly in a short time and remained at lower concentrations until the end of the sea fog event. The nss-SO_4^{2-} concentration showed a small decrease at the beginning of sea fog formation and remained at a high concentration during sea fog processes. MSA^-, which showed a strong correlation with sea salt ions, exhibited a similar decreasing pattern during sea fog events. These results suggest that sea salt ions, such as Na^+, Cl^-, Mg^{2+} and ss-SO_4^{2-}, were more likely to serve as fog condensation nuclei and could be removed by sea fog more effectively than nss-SO_4^{2-}. MSA^- combined with sea salt particles, which were likely to nucleate and be removed by sea fog. Different scavenging characteristics could be found during the same type of sea fog processes, which supports previous studies that reported that sea fog processes were very complicated (Gultepe et al., 2007; Biswas et al., 2008; Li et al., 2011). Air masses, wind speeds, and dense sea ice over the Arctic Ocean may be the factors influencing the changes in WSIs during the observation period in sea ice regions of the Arctic Ocean; while condensation may be the primary factor leading to the reduction of sea salt ions during the sea fog periods, and other factors like the presence of dense sea ice and long-range transport input may also affect the decreasing rate.

CRediT authorship contribution statement

Shuhui Zhao: Conceptualization, Methodology, Writing – original draft, Data curation, Funding acquisition. **Jinpei Yan:** Conceptualization, Writing – review & editing, Data curation, Supervision, Project administration, Funding acquisition. **Qi Lin:** Investigation, Methodology, Data curation. **Lei Yao:** Writing – review & editing. **Keyhong Park:** Writing – review & editing, Writing – review & editing, Funding acquisition. **Jinyoung Jung:** Writing – review & editing. **Liqi Chen:** Conceptualization, Supervision, Funding acquisition. **Suqing Xu:** Formal analysis, Sea ice data analysis. **Meiping Sun:** Formal analysis, Formal analysis, Statistical analysis. **Shanshan Wang:** Formal analysis, Raw data analysis. **Hang Yang:** Formal analysis, Raw data analysis. **Jun Shi:** Formal analysis, Raw data analysis. **Miming Zhang:** Resources. **Heng Sun:** Resources, The work presented here was carried out in collaboration with all authors.

Declaration of competing interest

The authors declare that they have no known competing financial interests or personal relationships that could have appeared to influence the work reported in this paper.

Acknowledgments

This study is Financially supported by the Project Sponsored by the Scientific Research Foundation of Third Institute of Oceanography, Ministry of Natural Resources (MNR, China), NO. 2019024, National Natural Science Foundation of China (No.41941014), Chinese Projects for Investigations and Assessments of the Arctic and Antarctica (CHINARE2017-2020), Qingdao National Laboratory for Marine Science and Technology, China (No. QNLM2016ORP0109), the Natural Science Foundation of Fujian Province, China (No. 2019J01120), the fellowship

of China Postdoctoral Science Foundation (2021M693779). We thank the Chinese Arctic and Antarctic Administration (CAA) of State Oceanic Administration, China (SOA, China), the crew of R/V Xue Long for support with field operations, and the data/samples collected by the 8th Chinese National Arctic Research Expedition (CHINARE). We also thank the Korea Polar Research Institute (KOPRI, South Korea) Asian Polar Science Fellowship Program support for the research collaboration opportunities and partially supported by Korea-Arctic Ocean Warming and Response of Ecosystem project (K-AWARE, KOPRI, 1525011760) funded by the MOF, South Korea. The authors gratefully acknowledge Zhangjia Instrument Company Limited for the IGAC data analysis.

Appendix A. Supplementary data

Supplementary data to this article can be found online at https://doi.org/10.1016/j.atmosenv.2022.118943.

References

Aikawa, M., Hiraki, T., Suzuki, M., Tamaki, M., Kasahara, M., 2007. Separate chemical characterizations of fog water, aerosol, and gas before, during, and after fog events near an industrialized area in Japan. Atmos. Environ. 41 (9), 1950–1959.

Albu, M., Barnes, I., Becker, K.H., Patroescu-Klotz, I., Mocanu, R., Benter, T., 2006. Rate coefficients for the gas-phase reaction of OH radicals with dimethyl sulfide: temperature and O_2 partial pressure dependence. Phys. Chem. Chem. Phys. 8, 728–736.

Barnes, I., Hjorth, J., Mihalopoulos, N., 2006. Dimethyl sulfide and dimethyl sulfoxide and their oxidation in the atmosphere. Chem. Rev. 106, 940–975.

Bates, T.S., Calhoun, J.A., Quinn, P.K., 1992. Variations in the methanesulfonate to sulfate molar ratio in submicrometer marine aerosol particles. J. Geophys. Res. 97, 9859–9865.

Biswas, K.F., Ghauri, B.M., Husain, L., 2008. Gaseous and aerosol pollutants during fog and clear episodes in South Asian urban atmosphere. Atmos. Environ. 42, 7775–7785.

Bott, A., 1991. On the influence of the physico-chemical properties of aerosols on the life cycle of radiation fogs, Bound. Layer Meteor 56, 1–31.

Brege, M., Paglione, M., Gilardoni, S., Decesari, S., Facchini, M.C., Mazzoleni, L.R., 2018. Molecular insights on aging and aqueous-phase processing from ambient biomass burning emissions-influenced po valley fog and aerosol. Atmos. Chem. Phys. 18 (17), 13197–13214.

Castebrunet, H., Martinerie, P., Genthon, C., Cosme, E., 2009. A three-dimensional model study of methanesulphonic acid to non sea salt sulphate ratio at mid and high-southern latitudes. Atmos. Chem. Phys. 9, 9449–9469.

Charlson, R.J., Lovelock, J.E., Andreae, M.O., Warren, S.G., 1987. Oceanic phytoplankton, atmospheric sulphur, cloud albedo, and climate. Nature 326, 655–661.

Chen, Z., Wei, L., Li, Z., Liu, K., Ding, M., 2019. Sea fog characteristics over the Arctic pack ice in summer 2017. Mar. Forecasts 36 (2), 77–87 (in Chinese).

Chen, C.L., Chen, T.Y., Hung, H.M., Tsai, P.W., Chou, C.C.K., Chen, W.N., 2021. The influence of upslope fog on hygroscopicity and chemical composition of aerosols at a forest site in Taiwan. Atmos. Environ. 246 https://doi.org/10.1016/j.atmosenv.2020.118150.

Cotton, W.R., Anthes, R.A., 1989. Fogs and Stratocumulus clouds. Storm and cloud dynamics, 44. Academic Press, San Diego, pp. 303–367. International geophysics series.

Deser, C., Tomas, R., Alexander, M., Lawrence, D., 2010. The seasonal atmospheric response to projected Arctic sea ice loss in the late 21st century. J. Clim. 23 (2), 333–351.

Draxler, R.R., Rolph, G.D., 2003. HYSPLIT (Hybrid Single-Particle Lagrangian Integrated Trajectory) Model Access via NOAA ARL READY Website. NOAA Air Resources Laboratory, Silver Spring, MD. http://www.arl.noaa.gov/ready/hysplit4.html.

Eastman, R., Warren, S.G., 2010. Arctic cloud changes from surface and satellite observations. J. Clim. 23 (15), 4233–4242.

Exton, H.J., Latham, J., Park, P.M., Smith, M.H., Allan, R.R., 2010. The production and dispersal of maritime aerosol. Oceanic Whitecaps. Springer Netherlands 2 (469), 817–837. https://doi.org/10.1007/978-94-009-4668-2_17.

Fahey, K.M., Pandis, S.N., Collett Jr., J.L., Herckes, P., 2005. The influence of size-dependent droplet composition on pollutant processing by fogs. Atmos. Environ. 39, 4561–4574.

Fan, S.X., Huang, H.L., Gu, K.H., Li, H.S., Fan, Y., 2010. Effect of fog process on the size distribution of polycyclic aromatic hydrocarbons in the atmospheric aerosol PM10. Chem. J. Chin. Univ. (Chin. Ed.) 31 (12), 2375–2382.

Gilardoni, S., Massoli, P., Giulianelli, L., Rinaldi, M., Paglione, M., Pollini, F., et al., 2014. Fog scavenging of organic and inorganic aerosol in the Po Valley. Atmos. Chem. Phys. 14 (13), 6967–6981. https://doi.org/10.5194/acp-14-6967-2014.

Gilson, G.F., Jiskoot, H., Cassano, J.J., Gultepe, I., James, T.D., 2018. The thermodynamic structure of arctic coastal fog occurring during the melt season over East Greenland. Boundary-Layer Meteorol. 168, 443–467.

Gultepe, I., Tardif, R., Michaelides, S.C., Cermak, J., Bott, A., Bendix, J., Müller, M.D., Pagowski, M., Hansen, B., Ellrod, G., Jacobs, W., Toth, G., Cober, S.G., 2007. Fog research: a review of past achievements and future perspectives. Pure Appl. Geophys. 164, 1121–1159.

Hallberg, A., Orgen, J.A., 1992. Phase partitioning for different aerosol species in fog. Tellus B 44, 545–555.

Heintzenberg, J., Cereceda-Balic, F., Vidal, V., Leck, C., 2016. Scavenging of black carbon in Chilean coastal fogs. Sci. Total Environ. 541, 341–347. https://doi.org/10.1016/j.scitotenv.2015.09.057.

Hynes, A.J., Wine, P.H., Semmes, D.H., 1986. Kinetics and mechanism of hydroxyl reactions with organic sulfides. J. Phys. Chem. 90, 4148–4156.

Ian, B., Jeremy, P., Innocent, K., Harri, K., Sami, R., 2018. Aerosol–fog interaction and the transition to well-mixed radiation fog. Atmos. Chem. Phys. 18 (11), 7827–7840.

IPCC, 2013. Summary for policymakers. In: Stocker, T.F., Qin, D., Plattner, G.-K., Tignor, M., Allen, S.K., Boschung, J., Nauels, A., Xia, Y., BexV, MidgleyPM. (Eds.), Climate Change 2013: the Physical Science Basis. Contribution of Working Group I to the Fifth Assessment Report of the Intergovernmental Panel on Climate Change. Cambridge University Press, Cambridge, pp. 1–30.

Jia, X., Quan, J., Zheng, Z., Liu, X., Liu, Q., He, H., Liu, Y., 2019. Impacts of anthropogenic aerosols on fog in North China Plain. J. Geophys. Res. Atmos. 124, 252–265. https://doi.org/10.1029/2018JD029437.

Jung, J., Furutani, H., Uematsu, M., Kim, S., Yoon, S., 2013. Atmospheric inorganic nitrogen input via dry, wet, and sea fog deposition to the subarctic western North Pacific Ocean. Atmos. Chem. Phys. 13 (1), 411–428. https://doi.org/10.5194/acp-13-411-2013.

Jung, J., Furutani, H., Uematsu, M., Park, J., 2014. Distributions of atmospheric non-sea-salt sulfate and methanesulfonic acid over the Pacific Ocean between 48°N and 55°S during summer. Atmos. Environ. 99, 374–384.

Jung, J., Choi, Y., Wong, D.C., Nelson, D., Lee, S., 2021. Role of sea fog over the yellow sea on air quality with the direct effect of aerosols. J. Geophys. Res. Atmos. 126 (5) https://doi.org/10.1029/2020jd033498.

Koračin, D., Dorman, C.E., 2017. Marine Fog: Challenges and Advancements in Observations, Modeling, and Forecasting. Springer International Publishing, San Diego, CA.

Koračin, D., Lewis, J., Thompson, W.T., Dorman, C.E., Businger, J.A., 2001. Transition of stratus into fog along the California coast: observations and modeling. J. Atmos. Sci. 58 (13), 1714–1731.

Lange, R., Dall'Osto, M., Wex, H., Skov, H., Massling, A., 2019. Large summer contribution of organic biogenic aerosols to arctic cloud condensation nuclei. Geophys. Res. Lett. 46, 11500–11509.

Laskin, A., Gaspar, D.J., Wang, W., Hunt, S.W., Cowin, J.P., Colson, S.D., Finlayson-Pitts, B.J., 2003. Reactions at interfaces as a source of sulfate formation in sea-salt particles. Science 301, 340–344.

Leck, C., Bigg, E.K., 1999. Aerosol production over remote marine areas - a new route. Geophys. Res. Lett. 26 (23), 3577–3580. https://doi.org/10.1029/1999gl010807.

Li, P., Li, X., Yang, C., Wang, X., Chen, J., Collett, J.L., 2011. Fog water chemistry in Shanghai. Atmos. Environ. 45, 4034–4041.

Li, K., Jin, H., Zhao, X., Zhuang, Y., Ji, Z., Zhang, Y., Chen, J., 2020. Sources and degradation of organic matter in the Bering Sea and the western Arctic Ocean: implication from fatty acids. Hai Yang Xue Bao 42 (10), 14–27. https://doi.org/10.3969/j.issn.0253−4193.2020.10.002, 2020 (In chinese).

Liu, Z., Chen, J., Liu, Y., Bai, Y., Zhang, H., Gao, S., Li, H., Lu, Y., 2011. The size-fractionated chlorophyll a and primary productivity in the surveyed area of the western Arctic Ocean during the summer of 2008. Acta Oceanol. Sin. 33 (2), 124–133.

Lovelock, J.E., Maggs, R.J., Rasmussen, R.A., 1972. Atmospheric dimethyl sulphide and the natural sulphur cycle. Nature 237, 452–453.

May, N., Quinn, P., McNamara, S., Pratt, K., 2016. Multiyear study of the dependence of sea salt aerosol on wind speed and sea ice conditions in the coastal Arctic. J. Geophys. Res. Atmos. 121 (15), 9208–9219.

Millero, F.J., Sohn, M.L., 1992. Chemical Oceanography. CRC Press, Boca Raton, Fla, p. 531.

Mohan, M., Payra, S., 2006. Relation between fog formation and accumulation mode aerosols in urban environment of megacity Delhi. Indian J. Environ. Protect. 26, 294–300.

Mukherjee, P., Marsay, C.M., Yu, S., Buck, C.S., Gao, Y., 2021. Concentrations and size-distributions of water-soluble inorganic and organic species on aerosols over the arctic ocean observed during the US GEOTRACES Western Arctic Cruise GN01. Atmos. Environ. 261, 118569.

Niu, F., Li, Z., Li, C., Lee, K.H., Wang, M., 2010. Increase of wintertime fog in China: potential impacts of weakening of the Eastern Asian monsoon circulation and increasing aerosol loading. J. Geophys. Res. 115, D00K20 https://doi.org/10.1029/2009JD013484.

Palm, S.P., Strey, S.T., Spinhirne, J., Markus, T., 2010. Influence of Arctic sea ice extent on polar cloud fraction and vertical structure and implications for regional climate. J. Geophys. Res. 115, D21209 https://doi.org/10.1029/2010JD013900.

Pant, V., Deshpande, C.G., Kamra, A.K., 2010. Changes in concentration and size distribution of aerosols during fog over the south Indian ocean. J. Earth Syst. Sci. 119 (4), 479–487.

Read, K.A., Lewis, A.C., Bauguitte, S., Rankin, A.M., Salmon, R.A., Wolff, E.W., Saiz-Lopez, A., Bloss, W.J., Heard, D.E., Lee, J.D., Plane, J.M.C., 2008. DMS and MSA measurements in the Antarctic Boundary Layer: impact of BrO on MSA production. Atmos. Chem. Phys. 8, 2985–2997.

Sasakawa, M., Uematsu, M., 2002. Chemical composition of aerosol, sea fog, and rainwater in the marine boundary layer of the northwestern North Pacific and its marginal seas. J. Geophys. Res. 107 (D24), 4783. https://doi.org/10.1029/2001JD001004.

Sasakawa, M., Uematsu, M., 2005. Relative contribution of chemical composition to acidification of sea fog (stratus) over the northern north pacific and its marginal seas. Atmos. Environ. 39 (7), 1357–1362.

Sasakawa, M., Ooki, A., Uematsu, M., 2003. Aerosol size distribution during sea fog and its scavenge process of chemical substances over the northwestern North Pacific. J. Geophys. Res. 108 (D3), 4120. https://doi.org/10.1029/2002JD002329.

Sheng, L.F., Liang, W.F., Wen-Jun, Q.U., Luo, K., 2011. Relationship of aerosol size distribution and visibility in a sea fog. Period. Ocean Univ. China 41 (6), 1–8 (In Chinese).

Shin, D., Kim, J.H., 2018. A new application of unsupervised learning to nighttime sea fog detection. Asia-Pac. J Atmos. Sci. 54, 527–544.

Spreen, G., Kaleschke, L., Heygster, G., 2008. Sea ice remote sensing using AMSR-E 89 GHz channels. J. Geophys. Res. 113, C02S03.

Springer, A.M., Mcroy, C.P., Flint, M.V., 1996. The Bering Sea Green Belt: shelf-edge processes and ecosystem production. Fish. Oceanogr. 5, 205–223.

Tian, M., Wang, H.B., Chen, Y., Zhang, L.M., Shi, G.M., Liu, Y., Yu, J.Y., Zhai, C.Z., Wang, J., Yang, F.M., 2017. Highly time-resolved characterization of water-soluble inorganic ions in $PM_{2.5}$ in a humid and acidic mega city in Sichuan basin. China. Sci. Total Environ. 580, 224–234.

Tian, Y., Pan, X., Yan, J., Lin, Q., Sun, Y., Li, M., Xie, C., Uno, I., Liu, H., Wang, Z., 2019. Size distribution and depolarization properties of aerosol particles over the northwest pacific and arctic ocean from shipborne measurements during an R/V Xuelong cruise. Environ. Sci. Technol. 53 (14), 7984–7995.

Tjernström, M., Birch, C.E., Brooks, I.M., Shupe, M.D., Persson, P.O.G., Sedlar, J., Mauritsen, T., Leck, C., Paatero, J., Szczodrak, M., Wheeler, C.R., 2012. Meteorological conditions in the central arctic summer during the arctic summer cloud ocean study (ASCOS). Atmos. Chem. Phys. 12 (15), 6863–6889.

Tjernström, M., Shupe, M.D., Brooks, I.M., Persson, P.O.G., Prytherch, J., Salisbury, D.J., Sedlar, J., Achtert, P., Brooks, B.J., Johnston, P.E., Sotiropoulou, G., Wolfe, D., 2015. Warm-air advection, air mass transformation and fog causes rapid ice melt. Geophys. Res. Lett. 42, 5594–5602.

Tsai, I.C., Hsieh, P.R., Cheung, H.C., Chou, C.K., 2021. Aerosol impacts on fog microphysics over the western side of Taiwan Strait in April from 2015 to 2017. Atmos. Environ. 262, 118523.

Vavrus, S., Holland, M.M., Bailey, D.A., 2011. Changes in Arctic clouds during intervals of rapid sea ice loss. Clim. Dynam. 36 (7–8), 1475–1489.

Wang, B.-H., 1985. Distributions and variations of sea fog in the world. In: Sea Fog. China Ocean Press, pp. 51–90.

Yan, J., Jung, J., Lin, Q., Zhang, M., Xu, S., Zhao, S., 2020a. Effect of sea ice retreat on marine aerosol emissions in the Southern Ocean, Antarctica. Sci. Total Environ. 745, 140773.

Yan, J., Jung, J., Zhang, M., Bianchi, F., Tham, Y.J., Xu, S., Lin, Q., Zhao, S., Li, L., Chen, L., 2020b. Uptake selectivity of methanesulfonic acid (MSA) on fine particles over polynya regions of the Ross Sea, Antarctica. Atmos. Chem. Phys. 20 (5), 3259–3271.

Yang, Y., Gao, S., 2020. The impact of turbulent diffusion driven by fog-top cooling on sea fog development. J. Geophys. Res. Atmos. 125 https://doi.org/10.1029/2019JD031562 e2019JD031562.

Yao, X., Fang, M., Chan K., C., 2003. The size dependence of chloride depletion in fine and coarse sea-salt particles. Atmos. Environ. 37, 743–751.

Young, L.H., Li, C.H., Lin, M.Y., Hwang, B.F., Hsu, H.T., Chen, Y.C., Jung, C.R., Chen, K. C., Cheng, D.H., Wang, V.S., 2016. Field performance of a semi-continuous monitor for ambient $PM_{2.5}$ water-soluble inorganic ions and gases at a suburban site. Atmos. Environ. 144, 376–388.

Yu, C., Yan, J., Zhang, H., Lin, Q., Zheng, H., Zhao, S., Zhong, X., Zhao, S., Zhang, M., Chen, L., 2021. Chemical characteristics of sulfur-containing aerosol particles across the western North Pacific and the Arctic Ocean. Atmos. Res. 253, 105480.

Yu, C., Yan, J., Zhang, H., Lin, Q., Zheng, H., Zhong, X., et al., 2020. Characteristics of aerosol WSI with high-time-resolution observation over Arctic Ocean. Earth Space Sci. 7 https://doi.org/10.1029/2020EA001227 e2020EA001227.

Yue, Y., Niu, S., Zhao, L., Zhang, Y., Xu, F., 2012. Chemical composition of sea fog water along the south China sea. Pure Appl. Geophys. 169, 2231–2249.

Yue, Y., Niu, S., Zhao, L., Zhang, Y., Xu, F., 2014. The influences of macro- and microphysical characteristics of sea-fog on fog-water chemical composition. Adv. Atmos. Sci. 31, 624–636.

Yuskiewicz, B.A., Orsini, D., Stratmann, F., Wendisch, M., Wiedensohler, A., Heintzenberg, J., Martinsson, B., Frank, G., Wobrock, W., Schell, D., 1998. Changes in submicrometer particle distributions and light scattering during haze and fog events in a highly polluted environment. Contrib. Atmos. Phys. 71, 33–45.